ficients were refined for non-hydrogen cation atoms, and group isotropic thermal parameters were varied for the anion and hydrogen atoms. The triflate was refined as three rigid groups with the site occupancy of each independently varied.[51] Successful convergence was indicated by the maximum shift/error for the last cycle. The highest residual electron density located in the final difference Fourier map was in the vicinity of the disordered triflate molecule. A final analysis of variance between observed and calculated structure factors showed no apparent systematic errors. Atomic coordinates are presented in Table V.

(51) CSD entry TFMSUL (oxonium trifluoromethanesulfonate): Spencer, J. B.; Lundgren, J. O. *Acta Crystallogr.* **1973**, *B29*, 1923.

Acknowledgment. This research was supported by the National Science Foundation.

Registry No. **1**, 139584-16-0; **1**·CH_2Cl_2·PhMe, 139584-23-9; **2**, 139584-18-2; $CpRu(PPh_3)_2SeH$, 139606-50-1; $CpRu(PPh_3)_2Cl$, 32993-05-8; $(Me_4N)SeH$, 139584-19-3; $(MeCp)Ru(PPh_3)_2SeH$, 124858-03-3; $(MeCp)Ru(PPh_3)_2Cl$, 55272-36-1; $[CpRu(PPh_3)]_2Se_4(OTf)_2$, 139584-21-7; $[(MeCp)Ru(PPh_3)]_2Se_4$, 139584-22-8; $(MeCp)_4Ru_4Se_4$, 124858-08-8; $(C_6H_5)_3CBF_4$, 341-02-6.

Supplementary Material Available: For **1** and **2**, tables of thermal parameters, complete positional parameters, bond angles, and bond distances (18 pages); tables of structure factors (47 pages). Ordering information is given on any current masthead page.

Contribution from the Department of Chemistry,
Texas A&M University, College Station, Texas 77843-3255

Semilocalized Bonding Schemes in Extended Systems: Orbital Localization in Y_2Cl_3 and Interstitial Derivatives

Kyeong Ae Yee and Timothy Hughbanks*

Received September 5, 1991

A semilocalized description of bonding in extended metal–metal-bonded systems is described for the prototype title compounds. Beginning with calculated band orbitals, we explicitly construct localized orbitals (Wannier functions) for the metal–metal-bonding orbitals of a M_6X_{12} cluster and the Y_2Cl_3 chain compound. Face-localized three-center bond orbitals for a Zr_6Cl_{18} cluster are remarkably similar to the HOMO for a $(Zr_6Cl_{12}H_7)Cl_6^{3-}$ cluster in which hydrogens cap seven of eight Zr_6 cluster faces. The $(Zr_6Cl_{12}H_7)Cl_6^{3-}$ cluster was chosen to model $(Th_6Br^i_{12}H_7)Br^{a-a}_{6/2}$, reported recently by Simon and co-workers. A semilocalized bonding picture for semiconductors with the Gd_2Cl_3 structure type is constructed, providing clarification of both structure–property relationships and trends in interstitial chemistry of these compounds. For the metal–metal bonding, a scheme with two 4c–2e bonds and one 2c–2e bond per cell is extracted from the band structure. The insertion of hydrogens into the tetrahedral interstices of these chains (to form structures of the β-Y_2Cl_3N type) is seen to be plausible and chains formulated as $Y_4Cl_6H_2^{2+}$ are electronically viable.

Introduction

Local Orbitals for Clusters. There are several reasons for the difficulty with which molecular and solid-state inorganic chemists have difficulty communicating. Among the most important of these is the more practiced eye of the solid-state chemists in recognizing the order within extended solid-state structures. But this advantage is often negated by the lack of even qualitatively correct ways of describing bonding in solids within a localized framework. There are a number of reasons for pursuing useful local bonding representations, among them are (i) to offer experimentalists more guidance than is generally given by computational theory. Explanations for materials' properties that boil down to statements which assure us that "its in the band structure" are at best useful only for particular compounds for which computations have been carried out. Uncovering a localized description in the electronic structure can greatly aid in analyzing structurally similar materials and therefore aid in formulating synthetic goals. (ii) Local descriptions will provide a way for chemists to recognize *explicit* structure–property relationships that are a crucial prerequisite if we are to develop the ability to control properties. (iii) Understanding of the structural and reaction chemistry of the solids under investigation will inevitably be enhanced. Chemistry deals with inherently local phenomena; bonds are clearly made and broken *locally*. If appropriate analogies are to be drawn with the chemistry of molecules, then we must be able to compare the local electronic structure of molecules and solids.

Cluster compounds can serve to illustrate a way in which localized bonding can be extracted from delocalized representations. It has been known for some time that metal–metal bonding in octahedral clusters such as $Nb_6Cl_{12}^{2+}$ and $Mo_6Cl_8^{4+}$, in which nonmetals respectively cap the octahedron's edges and faces, could be understood using localized orbitals.[1] In the latter case 12 metal-based electron pairs may be viewed as localized in 2c–2e bonds along the octahedral edges, and in the former case the cluster's 16 Nb–Nb bonding electrons occupy localized 3c–2e bonds in the eight cluster faces. The power of the localized bonding view is underlined by the recent synthesis of the remarkable compound $Th_6Br_{15}H_7$ (**1**).[2,3a] The clusters in this

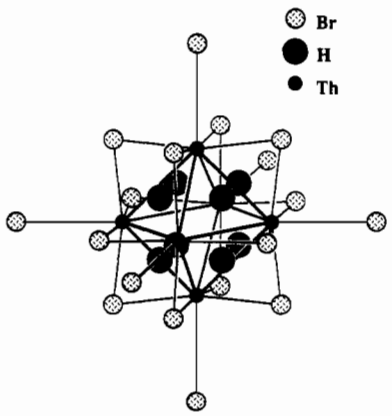

1

compound form a body-centered cubic array as in the Nb_6F_{15} structure type; $[(Th_6H_7)Br^i_{12}]^{3+}$ clusters are linked via linear

* To whom correspondence should be addressed.

(1) Kettle, S. F. A. *Theor. Chim. Acta* **1965**, *3*, 211.
(2) (a) Simon, A.; Böttcher, F.; Cockcroft, J. K. *Angew. Chem., Int. Ed. Engl.* **1991**, *30*, 101. (b) Böttcher, F.; Simon, A.; Kremer, R.; Buchkremer-Hermanns, H.; Cockroft, J. *Z. Anorg. Allg. Chem.* **1991**, *598/599*, 25.
(3) (a) Andersen, O. K. Cited in reference 2a. (b) Andersen, O. K.; Satpathy, S. *Basic Properties of Binary Oxides*; University of Seville: Seville, Spain, 1983.

0020-1669/92/1331-1620$03.00/0

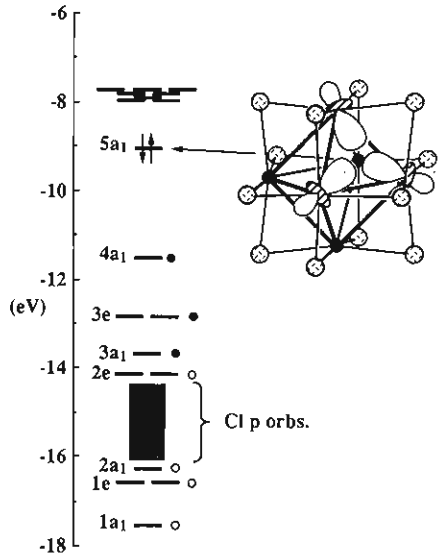

Figure 1. Molecular orbital diagram from a calculation on a model $Zr_6Cl_{18}H_7^{3-}$ cluster. The levels indicated by filled circles are those with predominantly Zr–H bonding character, and the shaded circles indicate levels with mixed Zr–H bonding and Cl p character.

bridging bromides to form simple cubic nets that interpenetrate to build up the final structure: $Th_6Br_{15}H_7 = [(Th_6H_7)Br^i_{12}]Br^a_3$. With the hydrogen electrons as part of the cluster bonding complement, the $[(Th_6H_7)Br^i_{12}]^{3+}$ cluster too has 16 bonding electrons.

Neutron diffraction analysis of deuterated samples reveals that seven D atoms are statistically disordered over the eight faces of the clusters. There are a number of ultimately equivalent ways to analyze the Th_6–H_7 bonding in these molecules, but perhaps the simplest is in terms of equivalent bond orbitals (BO's) of the cluster. The BO's are built up from the eight metal–metal-bonding molecular orbitals of the cluster and may be thought of as eight equivalent hybrids that are localized in each face of the cluster, as illustrated in **2**. These localized orbitals are in-phase com-

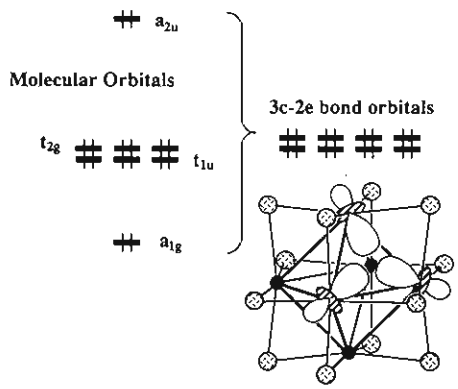

2

binations of a d orbital hybrid (the so-called d^4 orbitals of Andersen)[3b] from the surrounding three metal centers. Both the delocalized MO's and the eight face-localized BO's span the a_{1g}, t_{1u}, t_{2g}, and a_{2u} irreducible representations of the O_h group and give equivalent bonding pictures in that the electron density implied by either set of orbitals is identical.

A molecular orbital diagram from an extended Hückel calculation on a model $[Zr_6Cl^i_{12}Cl^a_6H_7]^{3-}$ cluster is shown in Figure 1. (MO calculations on the series of clusters $Th_6Cl^i_{12}Cl^a_6H_y$, y = 0–7, were reported by Simon and co-workers, but not with the purpose of constructing local orbitals.[2b]) For the calculation, the face in the $+x$, $+y$, $+z$ octant was left empty and the Zr–Zr and Zr–H bond lengths were set at 3.40 and 1.80 Å, respectively. The incomplete coverage of the cluster faces lowers the O_h symmetry of the cluster to C_{3v} with the C_3 axis normal to the empty face. A quick survey of the diagram in Figure 1 reveals that there are indeed seven orbitals with predominantly Zr–H-bonding character

Table I. Population Analysis for the Bond Orbitals of Zr_6Cl_{18} and the HOMO of $Zr_6Cl_{18}H_7^{3-}$

	% Zr_6Cl_{18}	% $Zr_6Cl_{18}H_7^{3-}$
[a] *top* Zr_3	78.2	79.1
[a] *bottom* Zr_3	7.3	9.4

[a] "Top" ("bottom") refers to the Zr_3 triangle which is (is not) part of the unprotonated face.

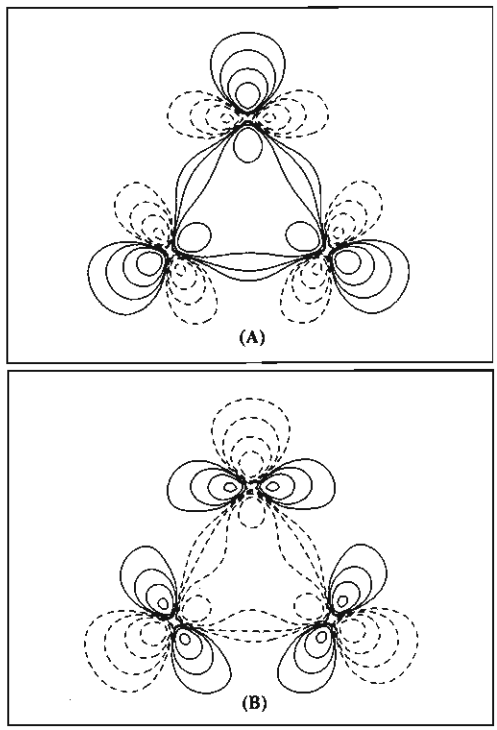

Figure 2. Contour plots for the local face-centered orbital of Zr_6Cl_{18} (A) compared to the HOMO of $Zr_6Cl_{18}H_7^{3-}$ (B). The open Zr_3 face defines the plane for the contour plots. Contours plotted are ±0.125, ±0.063, ±0.032, and ±0.016.

and one could use these to construct seven Zr_3H-bonding local orbitals, but more directly reminiscent of the bond orbital picture is the a_1 symmetry HOMO. For $Zr_6Cl_{18}H_7^{3-}$ this orbital is well localized in the open face and shows a very close resemblance to bond orbitals constructed for the unprotonated Zr_6Cl_{18} cluster. Table I shows the numerical results of Mulliken population analyses that demonstrate the extent of localization of the Zr_6Cl_{18} bond orbitals and the HOMO of $Zr_6Cl_{18}H_7^{3-}$; Figure 2 shows contour plots for each.

These results lead us to ask whether the eighth face of a Th_6 cluster might also be protonated in an appropriate cluster compound, for example in a $M_6X_{16}H_8$ phase or $M^I_2M_6X_{18}H_8$ (M = Zr or Th; X = halide). Such materials seem quite plausible from simple electron-counting considerations and are buttressed by the results seen here. An initially less obvious question is whether $Th_6Br_{18}H_7^{3-}$ clusters might be oxidized to leave the unprotonated face of the cluster without a three-center bond. The gap between the HOMO and the subjacent occupied levels in Figure 1 indicates that this is certainly a reasonable possibility—especially if a low-temperature solution-phase route to $Th_6Br_{18}H_7^{3-}$ can be managed via the dissolution of the known cluster phase, in chemistry analogous to the recently reported zirconium compounds.[4]

This example well illustrates the conceptual usefulness of a localized bonding scheme in describing molecular electronic structure. We believe that in condensed systems, a parallel approach may prove to be valuable because localized bonding schemes in metal-rich compounds have been difficult to intuit. In the remainder of this paper, we will see how the local electronic

(4) Rogel, F.; Corbett, J. D. *J. Am. Chem. Soc.* **1990**, *112*, 8198–8200.

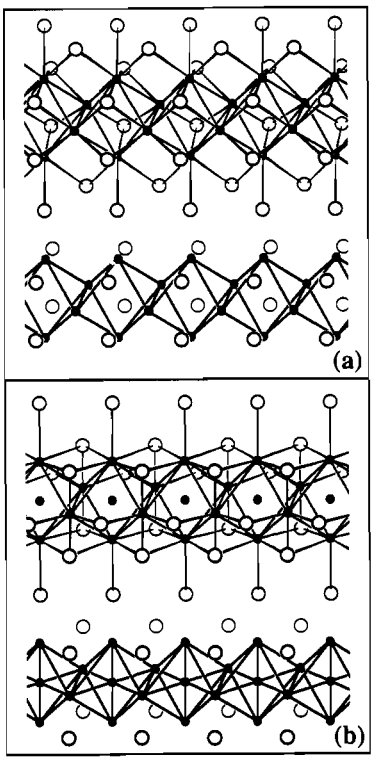

Figure 3. One-dimensional frameworks of edge-shared 6–8 and 6–12 condensed-cluster chains. Note the capping of the octahedral faces by ligands in the 6–8 condensed systems in (a) and the bridging of the octahedral edges in 6–12 condensed systems as shown in (b). Octahedra in the latter systems invariably are centered by interstitial atoms.

structure of structurally similar extended chain compounds is responsible for their different physical and chemical behavior. The extended Hückel tight-binding method is used for all calculations; parameters are given in the Appendix.[5,6]

Chains Built from Condensed M_6X_{12} and M_6X_8 Clusters. The structural characterization of gadolinium sesquichloride (Gd_2Cl_3) by Lokken and Corbett[7] and the preparation and characterization of the group IV monochlorides (ZrCl and HfCl)[8] gave us the first look at what has proven to be a rich area now known to be populated with a wide variety of metal-rich halides, oxides, and chalcogenides with low-dimensional metal–metal-bonded arrays. Among these, consider the one-dimensional framework structures shown in Figure 3. At top is the structural motif found in Y_2X_3 (X = Cl, Br; Gd_2Cl_3 type)[9a] and $Y_{10}I_{13}C_2$ ($(Y_4I_6)(Y_6I_7C_2)$);[9b] at bottom is an illustration of the chains found in materials such as Sc_5Cl_8Z ($(ScCl_2^+)(Sc_4Cl_6Z^-)$; Z = C, N), Sc_4Cl_6Z (Z = B, N), and Y_4I_5C (Gd_4I_5C type).[10-13] The metal–metal-bonded frameworks in both classes of compounds are quite similar and often described as the result of edge condensation of metal octahedra into infinite chains. Actually, only for oxide phases based on $^1_\infty[Mo_4O_6]$ chains are the octahedra in each structural class close to regular.[14-17] In electron poorer rare-earth compounds the octahedra are invariably stretched so that M–M contacts parallel to the chain axes are much longer than M–M contacts on the shared edges or those between the shared edges and the apices. (In Y_2Cl_3, the metal–metal contact along the shared edge is 3.27 Å, followed by 3.64–3.69-Å contacts between atoms in that edge and the apices. All Y–Y distances parallel to the chain axis are 3.83 Å.) For convenience, we will continue to discuss these structures with reference to the "octahedra" that are conventionally identified, even as we show that a focus on this structural feature may be inappropriate when it comes time to understanding the bonding.

The distinguishing structural features that separate the two classes of compounds in Figure 3 are the different positioning of the surrounding halide ligands and, in the second class (Figure 3b), the presence of interstitial atoms that invariably center the octahedra. In Figure 3a the halides are seen to cap the octahedral faces, just as in M_6X_8 clusters (such as $Mo_6Cl_8^{4+}$, $Re_6S_8^{2+}$, or $Nb_6I_8^{3+}$). Accordingly, these are often referred to as 6–8 condensed chains. In Figure 3b there are still three-coordinate halides but they sit over edges of the octahedra as in the M_6X_{12} cluster type (see above) and so this chain type is referred to as 6–12 condensed. It should be noted that many of the rare-earth 6–12 condensed phases were originally reported as binary compounds (*without* the interstitials);[18,19] subsequent investigations, cited above, have shown that in all well-characterized materials interstitials are present. Indeed, the recognition of the crucial role of interstitials in stabilizing these structures has lead to the subsequent development of this chemistry.[20-22] In contrast, with the exception of hydrogen, interstitial atoms have never been observed in the octahedral interstices of M_6X_8 clusters or 6–8 condensed compounds. The tetrahedral interstices of Y_2Cl_3 *can* be filled; the metal frameworks of β-M_2Cl_3N (M = Y, Gd) phases are virtually identical when the tetrahedral interstices are occupied by nitrogen—compare the lower illustration in Figure 3a with **3**, where interstitial nitrogens are shown as filled circles.[23]

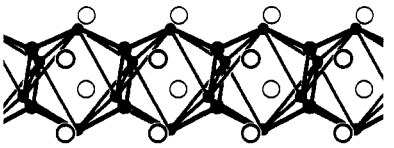

3

Of special interest to us is the contrast in electrical properties of these two classes of compounds. Resistivity measurements on Gd_2Cl_3 show it to be semiconducting with an estimated band gap of 0.85 eV. The photoelectron spectrum of Gd_2Cl_3 is consistent with the resistivity measurements and the electronic structural calculations.[24] Resistivity measurements on Y_2Cl_3 show that it has essentially the same band gap, and ^{89}Y NMR spectroscopy indicated paramagnetic shielding consistent with relatively electron-rich Y centers.[25] Band structure calculations indicate that the sesquichlorides have three low-lying, overlapping d bands, split off from the remainder of the d block and having a very small band width.[26] Since the sesquichlorides have 6 e available for metal–metal bonding per unit cell (e.g., Gd_2Cl_3 = $(Gd^{3+})_4(Cl^-)_6(e^-)_6$), the semiconducting behavior is consistent. Available

(5) Hoffmann, R.; Lipscomb, W. N. *J. Chem. Phys.* **1962**, *37*, 2872.
(6) Hoffmann, R. *J. Chem. Phys.* **1963**, *39*, 1397.
(7) Lokken, D. A.; Corbett, J. D. *Inorg. Chem.* **1973**, *12*, 556.
(8) (a) Ismailovich, A. S.; Troyanov, S. I.; Tsirel'nikov, V. I. *Russ. J. Inorg. Chem. (Engl. Transl.)* **1974**, *19*, 1597. (b) Troyanov, S. I.; Tsirel'nikov, V. I. *Russ. J. Inorg. Chem. (Engl. Transl.)* **1970**, *15*, 1762. (c) Struss, A. W.; Corbett, J. D. *Inorg. Chem.* **1970**, *9*, 1373. (d) Adolphson, D. G.; Corbett, J. D. *Inorg. Chem.* **1976**, *15*, 1820. (e) Daake, R. L.; Corbett, J. D. *Inorg. Chem.* **1977**, *16*, 2029.
(9) (a) Mattausch, H. J.; Hendricks, J. B.; Eger, R.; Corbett, J. D.; Simon, A. *Inorg. Chem.* **1980**, *19*, 2128. (b) Kauzlarich, S. M.; Payne, M. W.; Corbett, J. D. *Inorg. Chem.* **1990**, *29*, 3777.
(10) Hwu, S.-J.; Corbett, J. D. *J. Solid State Chem.* **1986**, *64*, 331.
(11) Hwu, S.-J.; Dudis, D. S.; Corbett, J. D. *Inorg. Chem.* **1987**, *26*, 469.
(12) Kauzlarich, S. M.; Hughbanks, T.; Corbett, J. D.; Klavins, P.; Shelton, R. N. *Inorg. Chem.* **1988**, *27*, 1791.
(13) Simon, A. *J. Solid State Chem.* **1985**, *57*, 2.
(14) Torardi, C. C.; McCarley, R. E. *J. Am. Chem. Soc.* **1979**, *101*, 1963.
(15) Torardi, C. C.; McCarley, R. E. *Inorg. Chem.* **1985**, *24*, 476.
(16) McCarley, R. E.; Lii, K.-W.; Edwards, P. A.; Brough, L. F. *J. Solid State Chem.* **1985**, *57*, 17.
(17) McCarley, R. E. *Polyhedron* **1986**, *5*, 51.
(18) Poeppelmeier, K. R.; Corbett, J. D. *J. Am. Chem. Soc.* **1978**, *100*, 5039.
(19) Simon, A. *Angew. Chem., Int. Ed. Engl.* **1981**, *20*, 1.
(20) Hughbanks, T. *Prog. Solid State Chem.* **1989**, *19*, 329.
(21) Simon, A. *Angew. Chem., Int. Ed. Engl.* **1988**, *27*, 160.
(22) Ziebarth, R. P.; Corbett, J. D. *Acc. Chem. Res.* **1989**, *22*, 256.
(23) Meyer, H.-J.; Jones, N. L.; Corbett, J. D. *Inorg. Chem.* **1989**, *28*, 2635.
(24) Ebbinghaus, G.; Simon, A.; Griffith, A. *Z. Naturforsch.* **1982**, *A37*, 564.
(25) Kremer, R. K.; Mattausch, H.; Simon, A.; Steuernagel, S.; Smith, M. E. *J. Solid State Chem.* **1991**, *95*, 000.
(26) Bullett, D. W. *Inorg. Chem.* **1985**, *24*, 3319.

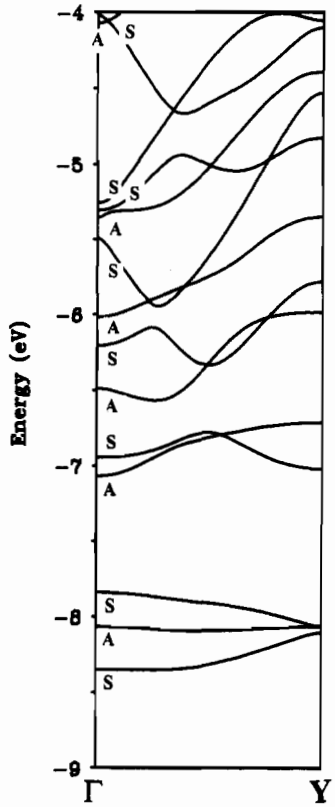

Figure 4. One-dimensional band structure of the Y_2Cl_3 model. The labels S (symmetric) and A (antisymmetric) refer to the crystal orbital symmetries with respect to a C_2 rotation about the chain propagation axis.

measurements of the 6–12 condensed materials indicate that they are conductors,[12] and band structure calculations indicate that these chain compounds should be conductors. Why the difference? Why do the M_2Cl_3Z (M = Y, Gd; Z = N) compounds bind nitrides in their tetrahedral holes[23] rather than the octahedral holes as for interstitials in Sc_4Cl_6Z (Z = B, N)? What is the structural–electronic relationship that governs the changes in chemical and physical properties of these very similar metal–metal-bonded networks? Electronic structure calculations have so far confirmed the facts—what we seek are explicit structure–property connections.

Bond Orbitals of the Y_2Cl_3 System. The band structure of Y_2Cl_3 is shown in Figure 4. The energy gap range shown includes those bands which have primarily Y 4d character; chloride 3s and 3p bands lie lower in energy and are not plotted. As mentioned above, the splitting of three d bands from the remainder of the d block is conspicuous. This result closely matches that obtained by Bullett for Gd_2Cl_3 using a tight-binding method.[26] Of the three occupied d bands, two are symmetric (S) and one is antisymmetric (A) with respect to the C_2 axis which coincides with the chain propagation axis.

In our approach to metal–metal bonding in this system, we construct local orbitals using a method quite analogous to that used to obtain bond orbitals for the M_6X_{12} cluster system discussed in the Introduction. Details of our procedures are discussed in the Appendix and in a previous paper,[27] but we make the following points here: (i) Just as for the relationship between bond orbitals and molecular orbitals in the cluster case, the local orbitals produce and electron density that is fully equivalent to that for the delocalized band orbitals from which the local orbitals are built. (ii) When bonding is discussed using local orbitals, one should recall the fact that identical orbitals are found in each unit cell of the crystal. For each band, there are as many delocalized band orbitals as there are unit cells in the crystal, but all are delocalized over the entire crystal.

(27) Yee, K. A.; Hughbanks, T. *Inorg. Chem.* **1991**, *30*, 2321.

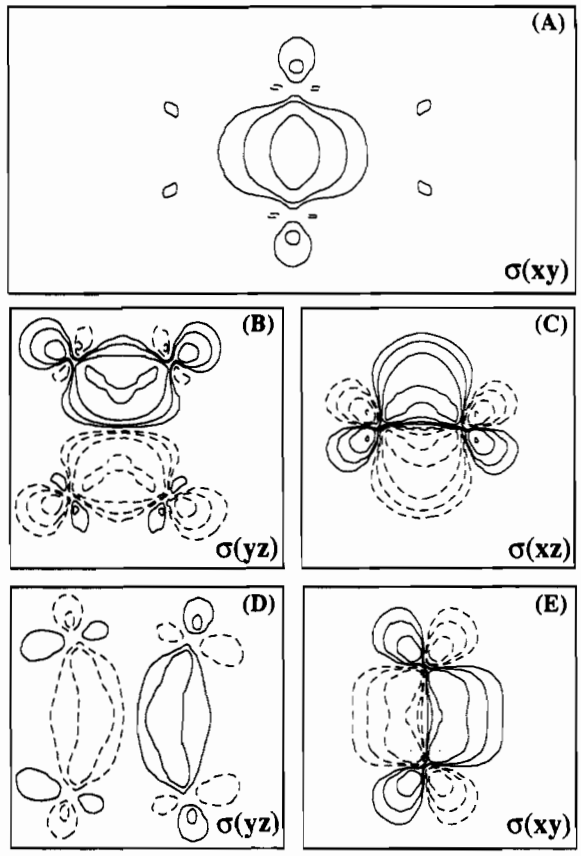

Figure 5. Wannier functions for each of three occupied bands of Y_2Cl_3: (A) 2c–2e S(σ) Wannier orbital derived from the lowest S symmetry band of Figure 4 (contours: ±0.125, ±0.0625, ±0.0325); (B) A(π) Wannier orbital built up from the crystal orbitals of the lowest lying A symmetry band of Figure 4 (contours plotted in the $\sigma(yz)$ plane—see 4—at ±0.100, ±0.050, ±0.025, ±0.0125); (C) same as in (B) with plots in the $\sigma(xz)$ plane; (D) S(π) Wannier orbital built up from the crystal orbitals of the second lowest lying S symmetry band of Figure 4 (contours plotted in the $\sigma(yz)$ plane at ±0.0625, ±0.031 25); (E) same as in (D) with plots at ±0.125, ±0.0625, ±0.0325, ±0.016 25 in the $\sigma(xy)$ plane.

Wannier functions for each of the three occupied bands are depicted in Figure 5. The lowest of the three bands has clear σ-bonding character between the pair of basal Y atoms. In this, our approach confirms the discussion of Bullett regarding the nature of this band.[25] For the remaining two bands, well-localized two-center bonds cannot be built. In fact, local orbitals constructed from each of the two remaining bands yield resultant orbitals that cannot be well localized on fewer than six centers. Schematic illustrations of these orbitals are shown in **4**, for the S and A

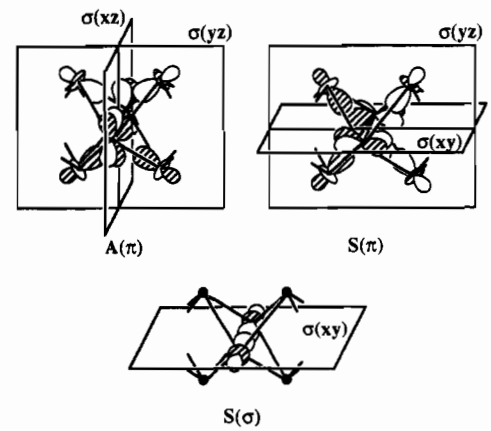

4

symmetry bands. The bottom picture in **4** shows the bond orbital for the lowest σ-bonding band. Both of the remaining orbitals

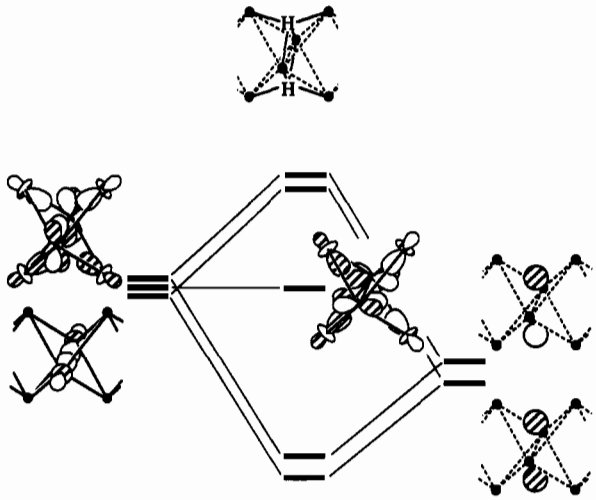

Figure 6. Diagram indicating the interaction between the occupied local orbitals of Y_2Cl_3 and hydrogen interstitials in the tetrahedral holes.

have π character with respect to bonding between the pair of basal metal centers but involve considerable apical–basal bonding as well.

All three of the local orbitals have C_{2h} point symmetry, and this reflects the symmetry about the midpoint of the bond between basal yttrium atoms. The local orbitals shown in **4** are very useful for understanding the interaction of the Y_2Cl_3 chain orbitals with interstitials placed in the tetrahedral interstices. Consider first the potential compound $Y_4H_2Cl_6$ in which hydrogens sit in the tetrahedral sites, as illustrated in **3**. To predict the fate of the valence bands for the chain when we add the hydrogens, we can simply examine the local orbitals in **4** and construct an interaction diagram using in-phase and out-of-phase combinations of the two hydrogen orbitals, as schematically shown in Figure 6. The two hydrogen 1s orbitals interact with only those two local orbitals that are symmetric with respect to the plane containing the two basal metals and the hydrogens themselves.

When the band structure diagram for $Y_4H_2Cl_6$ in Figure 7 is compared with the diagram for the Y_2Cl_3 chain in Figure 4, the effect of hydrogen in the tetrahedral interstices is easily understood. Since the S(π) local orbital is unperturbed in Figure 6, we expect one remaining low-lying Y–Y-bonding band in the band structure of the $Y_4H_2Cl_6$ chain. Indeed, when we construct a local Wannier orbital for the single low-lying band, the function closely resembles that plotted in Figure 5D,E. Just as the local orbital diagram of Figure 6 leads us to expect, the two other low-lying bands of Y_2Cl_3 are "absent" for the $Y_4H_2Cl_6$ chain. The bonding combination between these bands and the hydride orbitals lies at lower energy than our diagram's cutoff, and the antibonding counterparts move into and mix with the dense antibonding block at higher energy. Since one low-lying band remains, two additional electrons might be accommodated per unit cell; a system in which the chains are isoelectronic with the formulation $(Y^{3+})_4(Cl^-)_6(H^-)_2(e^-)_2$ = $Y_4Cl_6H_2^{2+}$ represents a plausible synthetic target.

We can see that the insertion of nitrogen atoms into the tetrahedral interstices should entirely eliminate any low-lying Y d bands because there are nitrogen p orbitals of the proper symmetry to interact with all three of the valence band local orbitals, and more. The possibility of a more electron-rich compound with the β-Y_2Cl_3N structure would seem to be remote, there are no low-lying d bands to accommodate the additional electrons.

The spirit of bond orbital construction does not require that individual localized orbitals display the symmetry of the system. Indeed, in the language of group theory, we may say that to construct local orbitals, we must take linear combinations of band orbitals that transform as irreducible representations of the crystal's translational subgroup; see the appendix, eq 3. (Just one of the meanings attached to k, the wavevector for the band orbitals, is that of a label for the translational subgroup.) There is no reason that we must stop with the two local orbitals shown in **4**, and we can obtain two identical well-localized 4c–2e bond orbitals by

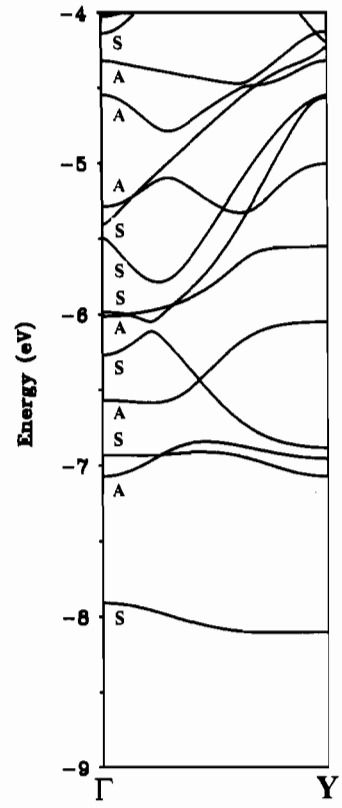

Figure 7. Band structure of the $Y_4Cl_6H_2^{2+}$ system. Notice that two bands, S(σ) and A(π), are no longer at low energy, having been pushed up by interaction with interstitial hydrogens. Comparison with Figure 4 shows that the S(π) band is virtually unperturbed.

taking combinations of the S(π) and A(π) orbitals. One of these bond orbitals is shown at right in **5**, along with a depiction of the

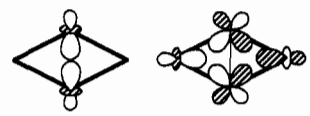

5

basal–basal σ bond. By examination of Figure 8 where we show calculated contours for the 4c–2e local orbital, the reader may see that the illustration at right in **5** is a quite reasonable representation.

We have come to a simple localized bonding scheme for the seemingly complex, metal–metal-bonded chains that thread the M_2X_3 structure. The scheme is entirely consistent with the delocalized band picture from which it is derived. For each unit cell, two electrons reside in each of three bond orbitals. As implied in **6**, the first is just a σ bond joining the basal metal atom pairs,

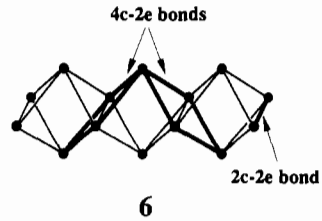

6

and the other two are identical 4c–2e bond orbitals delocalized over rhombuses that have the basal bond at their intersection.

Concluding Remarks

We have considered local orbitals for the metal–metal bonding in 6–12 clusters and 6–8 condensed cluster chains in some detail. An interesting general feature of the electron localization in these materials is the way in which metal–metal-bonding orbitals are efficiently localized in regions of the metal–metal-bonded network that are spatially removed from the place where the bridging or

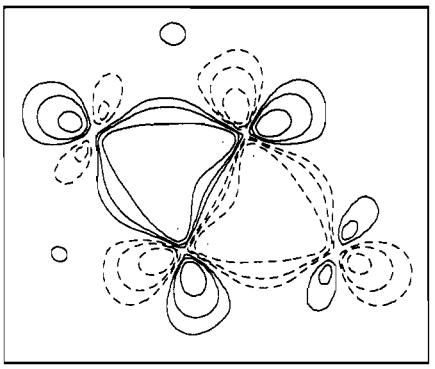

Figure 8. 4c–2e Wannier orbital for the Y_2Cl_3 system plotted in the plane of one of the rhombi indicated in 6. This orbital is schematically indicated in 5; contours are at ±0.125, ±0.0625, ±0.0325, ±0.01625.

Table II. Parameters for EH Calculations

	orbital	H_{ii}, eV	ζ_1[b]	ζ_2[b]	c_1[a]	c_2[a]
Zr	4d	−9.07	3.84	1.505	0.6213	0.5798
	5s	−8.76	1.82			
	5p	−5.07	1.78			
Y	4d	−6.80	1.56	3.55	0.8316	0.3041
	5s	−7.02	1.74			
	5p	−4.40	1.70			
Cl	3s	−30.0	2.36			
	3p	−15.0	2.04			
H	1s	−13.6	1.30			

[a] Coefficients used in double-ζ expansion. [b] Slater-type orbital exponents.

capping ligands are bound. For 6–12 clusters we have seen the familiar result that 3c–2e bonds are localized in the faces of the octahedral cluster while the ligands bridge the edges;[1] for the condensed 6–8 structure of Y_2Cl_3 the metal-based electrons similarly avoid the faces where the capping ligands are bound. All of this follows from the hybridization that the ligands and surrounding metals induce in each of the metal's atomic orbitals—no explicit e–e repulsion terms are included in extended Hückel calculations to bring this effect about, though presumably electrostatic factors would also favor this pattern of localization.

The question of whether, and where, interstitial atoms will be bound is more difficult to answer generally. It may be best to focus on the lowest lying orbitals that have nearly pure metal character. Formally, viewing the clusters or condensed cluster systems as acceptors and the interstitials as filled-shell donors (H^-, N^{3-}, etc.), we would expect strongest interaction of the filled donor levels with the lowest lying orbitals (bands) of the acceptors. In the present paper and in our previous work, the localized bonding picture has proven very useful in identifying the sites where the donor–acceptor overlap should be optimal, especially for extended systems.[27]

Acknowledgment. Partial support of this research was derived from a grant (No. 010366-111) by the Texas Advanced Research Program. We also acknowledge the National Science Foundation for its support through a Presidential Young Investigator Award (Grant DMR-8858151) and the Robert A. Welch Foundation for its support through Grant A-1132.

Appendix

Extended Hückel parameters appear in Table II. Structural parameters for Y_2Cl_3 were taken from crystallographic data, and for Sc_2Cl_3, from Sc_4Cl_6Z (Z = B, N). A one-dimensional model for the Y_2Cl_3 chain was constructed by replacing all Cl^a centers (which are in neighboring chains) with model "hydrides" such that the Y–"H" distance gave overlaps approximately equal to that for chlorine p orbitals; the "H" 1s orbital energy (H_{ii}) was taken to be −15.0 eV. This is a very satisfactory way of snipping lower dimensional pieces from cross-linked three-dimensional systems.[28] Structural parameters for $Zr_6Cl_{15}H_7$ were approximated by comparison with observed bond lengths in $Zr_6Cl_{15}Fe$, where the scale factor was obtained by comparison of the $Th_6Br_{15}H_7$ and $Th_6Br_{15}Fe$ structures.[2b] These parameters are subject to the simplications discussed in the text. Dispersion curves in Figures 4 and 7 are based on band structure calculations carried out using 100 k points in the one-dimensional Brillouin Zone. Wannier functions were constructed following the prescription outlined below. In all cases, the number of k points (N_k) in the entire first Brillouin zone for the band structure calculations must be large enough that the extent of localization of the Wannier functions is unaffected by increasing N_k. In practice this means that the Wannier function must be well localized within a radius, $r_0 \approx (a/2)(N_k)^{1/n}$, where a is a typical lattice parameter for the system and n is the dimensionality of the system (n = 1, 2, or 3). For the calculation of Wannier functions for Y_2Cl_3 and Sc_2Cl_3 we found it convenient to double the size of the one-dimensional unit cell so that an entire M_6 octahedron was contained within it. With this expanded cell, we performed a calculation using 10 k points in half of the zone. The other half of the zone simply yields complex conjugate wavefunctions which need not be calculated but for the purposes of estimating r_0 in the above formula, N_k = 20.

The Wannier functions are constructed from the crystal orbitals (CO's; the one-electron wave functions), and the CO's are in turn built up from symmetrized Bloch basis orbitals ($\chi_{i,\mathbf{k}}$):

$$\chi_{i,\mathbf{k}} = \frac{1}{\sqrt{N}}\sum_{\mathbf{R}} e^{i\mathbf{k}\cdot\mathbf{R}}\chi_i(\mathbf{r} - \mathbf{R}) \tag{1}$$

The displacement of a given unit cell from the origin is given by **R** and i is a label that runs over the list of atomic orbitals (AO's) in a unit cell. The CO's ($\phi_{\mathbf{k},n}$) are obtained from the linear combinations of the Bloch basis orbitals:

$$\phi_{\mathbf{k},n} = \sum_i c_{i,n}(\mathbf{k})\chi_{i,\mathbf{k}} \tag{2}$$

where n is the band index. A Wannier function is obtained for each band around lattice site **R** employing the prescription

$$\omega_n(\mathbf{r} - \mathbf{R}) = \frac{1}{\sqrt{N}}\sum_{\mathbf{k}}^{\mathrm{BZ}} e^{-i\mathbf{k}\cdot\mathbf{R}}\alpha_{\mathbf{k}}\phi_{\mathbf{k},n} \tag{3}$$

where $\alpha_{\mathbf{k}}$ is an undetermined phase factor. To construct localized bond orbitals, we first place a "probe" orbital in the appropriate location, such as a hydrogen 1s orbital in a tetrahedral hole for Y_2Cl_3, and determine the overlap between the probe orbital and the crystal orbital in question: $\langle\phi_{\mathrm{probe}}|\phi_{\mathbf{k},n}\rangle = |S|\exp(i\theta)$. The phase factor $\alpha_{\mathbf{k}}$ is chosen in order to make this overlap real and positive, we therefore take $\alpha_{\mathbf{k}} = \exp(-i\theta)$ so that $\langle\phi_{\mathrm{probe}}|\alpha_{\mathbf{k}}\phi_{\mathbf{k},n}\rangle = |S|$. The phase-shifted orbitals are then summed as in eq 3 to produce local orbitals that have maximum amplitude in the probe orbital location. The probe orbital can be changed to produce Wannier orbitals of different symmetry; for example, the A(π) orbital shown in Figure 5b,c results from the use of a probe p orbital placed at the midpoint of the Y_{basal}–Y_{basal} bond.

(28) Hughbanks, T.; Hoffmann, R. *J. Am. Chem. Soc.* **1983**, *105*, 1150.